Journal of the Maharaja Sayajirao University of Baroda
ISSN: 0025-0422

SOLAR PHOTOCATALYTIC DEGRADATION OF METHYLENE BLUE USING Sb-DOPED TiO_2 NANOPARTICLES

B.Y. Pagare Department of Chemistry, Shri Anand College, Pathardi, Ahmednagar, 414102, Maharashtra, India.

R. R. Bhosale Department of Chemistry, Arts, Science and Commerce College, Indapur, Pune, 413106, Maharashtra, India.

S. K. Narwade* Department of Chemistry, Shri Anand College, Pathardi, Ahmednagar, 414102, Maharashtra, India.

Abstract:
Sb-doped TiO_2 were synthesized by sol–gel process combined with surfactant incorporating method. The concentration level of Sb (III) additive was varied systematically from 1 to 11 wt.%. Wide structural and surface characterization of samples was carried out in order to establish a correlation between the effects of antimony incorporation on the TiO_2 photocatalytic properties. Results revealed that the anatase structure is highly stable for Sb/TiO_2 with enhancement in the surface area. UV–Vis diffuse reflectance spectra showed that this dopant was responsible for narrowing the band gap of TiO_2 and shifting its optical response from ultraviolet to visible-light region. The photocatalytic activity of the Sb/TiO_2 catalyst was evaluated in the decomposition of methylene blue solution under solar light irradiation with respect to the content of antimony on the catalyst surface. The results showed that the incorporation of antimony into the TiO_2 seems to enhance the photocatalytic activity of the samples, which is ascribed to the enlargement of specific surface area, photo generated carriers separation, light absorption, as well as the higher surface acidity. The photocatalytic efficiency and activity of the composites remained good, even after three cycles.
Keywords: Sb/TiO_2; Nanomaterials; Solar photocatalysis; Methylene blue.

Introduction:

Photocatalysis has emerged as an effective technique to decontaminate toxic and non-biodegradable environmental pollutants [1-2]. Among various functional metal oxides, TiO_2 is the most nontoxic, highly stable, cost effective, strong oxidant, and noncorrosive semiconductor, which make it more suitable choice for removing organic and inorganic contaminants from the environment [3-4]. The photochemical reactions proceed on a pure TiO_2 surface, when irradiated with ultraviolet light. This barricades the frequent and convenient use of TiO_2 photocatalyst. The increase in redox potential and decrease in the particle size is essential to enhance the photochemical reaction rates. Decreasing the particle size to nano scale, results in the larger surface area per unit mass. Reduction of band gap facilitates the catalyst to make use of solar and visible light energy, which makes it environmentally and electrically suitable photo catalyst [5]. Further, the anatase to rutile phase ratio is also an important factor in enhancing photo catalytic activity. The anatase phase is kinetically more stable and higher hydrophobicity of this phase increases the absorption of reactive species, while rutile phase scatters light which decreases its absorption power [6-7].

Recently, much attention has been paid in modifying TiO_2 to enhance its catalytic efficiency or expand its applicability under solar irradiation [8]. Different metallic [9] and nonmetallic dopants [10] have been doped to decrease the band gap and increase excitation life time of pure TiO_2. Mao et. al, used nitrogen dopant for the photo-oxidation of organic molecules in water [11]. Shamalah et. al, showed degradation of Brilliant Green dye with Zn and Cu-doped TiO_2 [12]. Moreover, many attempts have been carried out in direction of attaining high surface area photocatalysts to increase active sites by using the support materials like zeolites [13], HZSM-11 zeolite [14], Clinoptilolite [15] and silica–clay composite [16]. Zhang et. al. synthesized mixed platinum catalysts supported on various carbon nanomaterials [17]. The nano Ag/Pt and methyl violet co-doped catalyst was developed resulted in higher photodegradation activities towards various dyes [18]. Elham S. Baeissa investigated the removal of cyanide employing cobalt metal doped on TiO_2–SiO_2 nanoparticles [19]. Nano sheets of $Au/HTiNbO_5$ have also been synthesized by Hsin-Yu Lin, et. al to produce hydrogen from water splitting [20]. The important issue governing the efficiency of photocatalytic oxidative degradation is minimizing electron-hole recombination by maximizing the rate of interfacial electron transfer to capture the photogenerated electron and/or hole. Various n and p type photocatalysts are well documented in the literature. A Na-doped p-type flower-like ZnO photocatalyst (Na:ZnO) that is highly visible-light-sensitive in air at room temperature was synthesized by a continuous flow microreactor [21]. Rh-doped $BaTiO_3$ powder was prepared by the polymerized complex (PC) method, and the photocatalytic activity for H_2 evolution from water was examined. $BaTiO_3$ is a wide-gap n-type semiconductor having a band gap of 3.0 eV. Doping Rh species into the lattice of $BaTiO_3$ resulted in the formation of new absorption bands in visible light region [22]. Different p-type Cu_2O powders were prepared from electro deposition and subjected to analysis of their photocatalytic activity in water reduction [23]. Sb-doped catalyst on different supports has been synthesized previously [24-25]. However, they did not evaluate the effect of concentration level of Sb (III) on crystallite size, specific surface area and phase transformation and surface

acidity. The effect of variation of concentration of Sb (III) additive on the particle size and surface area of Sb-doped TiO_2 system is not reported in the literature so far.

In the present study highly pure and stable anatase Sb-doped TiO_2 nanopowders have been synthesized by sol-gel method at lower calcination temperature. The developed procedure is simple and low cost, which avoids the use of hazardous chemical compounds. The synthesized powders were structurally, morphologically and optically characterized and its photocatalytic properties studied under solar light irradiation.

2. Experimental details

2.1.1 Synthesis of Sb-doped TiO_2

In a typical procedure, 25 ml of titanium butoxide was hydrolyzed in 300 ml water containing 0.1M HNO_3 (10 ml) as a catalyst. The procedure was followed by the addition of 10% 10 ml of cationic surfactant cetyltrimethylammonium bromide. The solution was stirred vigoursly overnight to get peroxy sol. To obtain a composition of 1 wt.% Sb (III), a calculated amount of $SbCl_3$ was added to the above solution. The sol was stirred again for 5 h and then kept for aging. After keeping the sol for aging (5 days), it was concentrated and dried at 70°C. Finally, all the samples were calcined at 400°C, using muffle furnace for 2 h. Following this method, the various amounts of Sb (III) (0, 1, 3, 5, 7, 9, and 11 wt.%) were added to TiO_2.

2.1.2 Photocatalytic activity

Photocatalytic degradation of methylene blue (MB) was carried out by solar light irradiation. About 40 mg of photocatalyst was immersed into a 50 ml (50 ppm) of aqueous MB solution in closed cylindrical Pyrex bottles (100 ml). Prior to irradiation, the suspensions were magnetically stirred in the dark for 30 min to ensure establishment of an adsorption–desorption equilibrium among the photocatalyst, MB and atmospheric oxygen. All the experiments were carried out at the same conditions on May 2014 from 12.00 p.m. to 1.00 p.m. The average insolation of the solar irradiation was 25.28 W/m^2 measured by an UV irradiance meter at range of 375–475 nm. At a given irradiation time interval, 10 ml of the suspension was collected, and then filtered through a Millipore filter to separate the photocatalyst. The changes in MB concentration were analyzed by a UV–visible spectrophotometer and the absorption peak at 650 nm was recorded.

2.1.3 Characterization

X-ray powder diffraction (XRD) patterns have been recorded on a model D8 Bruker AXS with monochromatic Cu radiation (40 kV and 30 mA), over the 2θ collection range of 20-80°. Thermo gravimetric analysis (TG) and differential scanning calorimetric analysis (DSC) was carried out simultaneously in a static N_2 atmosphere, using a Netzsch STA 409 instrument. BET surface area measurements were carried out using a Quantachrome NOVA 1200 instrument. Surface morphology and elemental analysis of the samples were carried out using an energy dispersive spectrophotometer (EDS) (Jeol; JED-2300). The microscopic nanostructures were observed by transmission electron microscopy (TEM; FEI, Tecnai F30, HRTEM, FEG operated at 300 kV). To determine the acidity of the samples, ammonia TPD measurements in the range of 100-600°C were performed in a conventional flow-type apparatus at a heating rate of 10°C min^{-1} in a nitrogen atmosphere. The acidity determination was supported by the TGA studies using 2, 6-dimethylpyridine as a probe molecule. Previously activated samples were kept in a desiccators saturated with vapors of 2, 6-dimethylpyridine at room temperature for 24 h and then subjected to thermal analysis in N_2 atmosphere at a heating rate of 10°C min^{-1}. The fraction of weight loss in the range of 300-600°C was calculated and taken as a measure of Brönsted acidity of the samples. FT-IR spectra were recorded on a Shimadzu-8400 spectrometer in the range of 4000-500 cm-1. UV-Vis diffuse reflectance spectra (UV–Vis–DRS) were recorded in an air at room temperature in the wavelength range of 200–800 nm using a PE LAMBDA35 spectrophotometer.

3. Results and discussion

3.1 XRD analysis

To understand phase symmetry in the calcined samples, a systematic X-ray diffraction study was undertaken. Fig. 1(a–g) shows the XRD patterns of the pure TiO_2 and with different concentration levels of Sb (1, 3, 5, 7, 9 and 11wt.%) for Sb/TiO_2 system, respectively. Pure TiO_2 (Fig. 1(a)) shows two main peaks at 2□ =25.5 and 27.5, corresponding to (101) phase of anatase and (110) phase of rutile, respectively. In the case of Sb-doped TiO_2 (Fig. 1(b-g)), the rutile phase is □ 1%, which means metal-doping retards the transformation from anatase to rutile phase. Metal-doping of the TiO_2 stabilizes a well-crystallized pure anatase upon calcination at 400□C, in contrast with the simultaneous growth of the rutile phase observed for the pure TiO_2. The results are in good agreement with previous reports [26-27]**.** Further, all peaks measured by XRD analysis could be assigned to those of TiO_2 crystal. No peaks corresponding to the metal oxide is detected, suggesting that it exist as the amorphous phase without getting incorporated into the TiO_2 phase; that is, they are in a highly dispersed form on the surface. The peaks of TiO_2 have been slightly shifted due to solid solution of metal ion with TiO_2. The average particle sizes of the samples were calculated using Debye-Scherrer formula based on the XRD peak broadening analysis at 101 peaks, listed in Table 1. The particle size calculated from XRD data is as large as 9-22 nm for 1, 3, 7, 9 and 11 wt.% Sb-doped TiO_2 and as small as 6 nm for the 5 wt.% Sb-doped TiO_2. This apparent fall in the particle size (higher specific surface area) will ensure high photocatalytic activity for the 5 wt.% Sb-doped TiO_2 when it is used for photocatalytic applications.

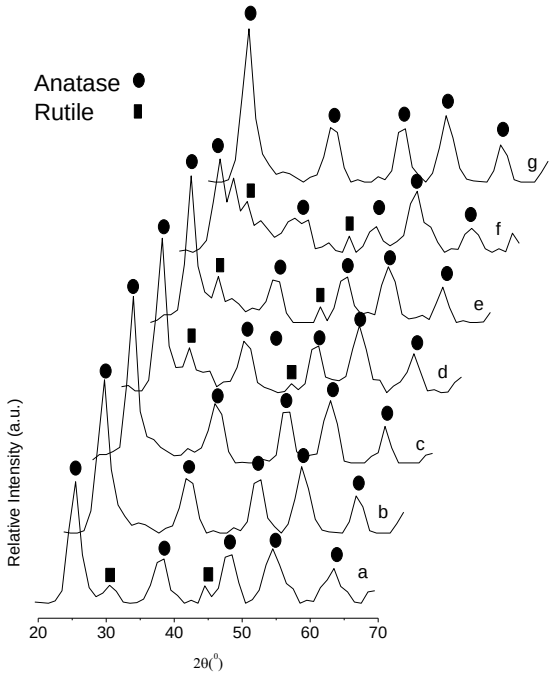

Fig. 1.(a–g) XRD of (a) Pure TiO_2, (b) 1 wt.% Sb/TiO_2, (c) 3 wt.% Sb/TiO_2, (d) 5 wt.% Sb/TiO_2, (e),7 wt.% Sb/TiO_2, (f) 9 wt.% Sb/TiO_2, (g) 11 wt.% Sb/TiO_2.

3.2. TEM and HRTEM analysis

In order to confirm the effect of metal incorporated samples on particle size and hence higher specific surface area of TiO_2 in the composite powders, the particle size of 3, 5 and 7 wt.% Sb-doped TiO_2 samples were observed using TEM.

Fig. 2(a-d) shows TEM and HRTEM images of 3, 5 and 7 wt.% Sb/TiO_2 samples and its corresponding Fourier transfer patterns (FTT) are also presented in the inset of figures. It can be seen that the particle size of composite samples with 3, 5 and 7 wt.% metal loading are about 6, 8 and 10 nm, respectively. The HRTEM images of samples (Fig. 3(c-d) also represent presence of highly crystalline nanoparticles with mesopores. The fringes appearing in the micrographs allow for the identification of the crystallographic spacing of the doped-TiO_2 nanocrystallites. The fringes most frequently observed correspond to the (101) crystal planes of TiO_2 anatase. The fringes of d = 3.7 Å observed in Fig. 3(c and d) match with (101) crystal planes of anatase TiO_2.

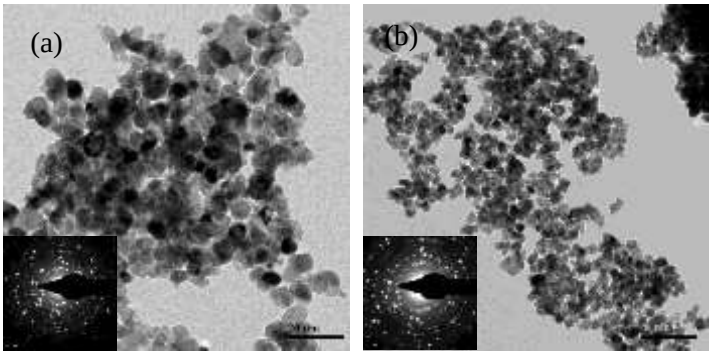

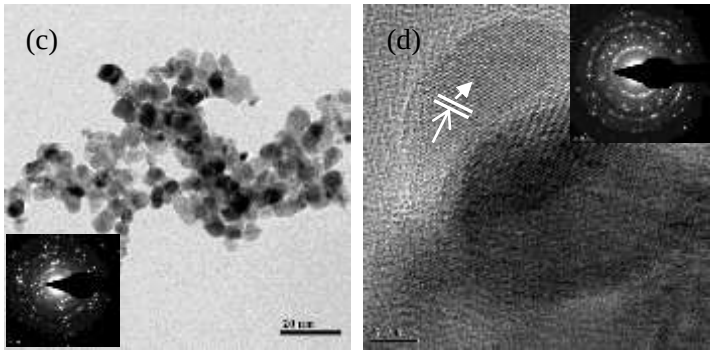

Fig. 2. (a–b) Typical TEM and HRTEM images of the (a) 3 wt% Sb/TiO_2, (b) 5 wt% Sb/TiO_2, (c) 7 wt% Sb/TiO_2.

3.3 BET surface area

All Sb-doped TiO_2 samples exhibit relatively high specific surface areas with respect to the pure TiO_2 (Table 1). The addition of Sb (III) metal ion cause a setback to the crystallization and sintering process, which is evident from the higher surface area of the samples in comparison with the pure TiO_2. [28]. The metal oxide species prevent the agglomeration of TiO_2 particles, resulting in a higher specific surface area. The surface area of the 5 wt.% Sb-doped TiO_2 sample calcined at 400°C is about 535.5 m^2/g. For the other samples, there is no much difference in the surface area.

Table 1. BET surface area, particle size, and surface acidity of synthesized samples

Samples	**BET surface area (m^2 g^{-1})**	**Particle size nm)**	**Total amount of ammonia desorbed (mmol g^{-1}), 100-600°C**	**Weight loss (%) of 2,6-DMP**
Pure TiO_2	34.00	12.61	0.6270	0.72
1 wt.% Sb/TiO_2	93.00	9.52	0.9521	5.11
3 wt.% Sb/TiO_2	435.7	6.01	0.9032	5.28
5 wt.% Sb/TiO_2	535.5	8.05	0.9362	4.65
7 wt.% Sb/TiO_2	516.0	10.03	0.9437	5.32
9 wt.% Sb/TiO_2	278.0	18.54	1.0029	2.55
11 wt.% Sb/TiO_2	105.0	22.38	0.9362	2.41

3.3 UV–VIS DR spectral analysis

Fig. 3 shows UV–vis diffuse reflectance spectra (DRS) of the Sb/TiO_2 photocatalyst calcined at 400°C. The impact of Sb (III) doping on the band gap of TiO_2 was investigated and a progressive shift in the band gap toward red region is observed.

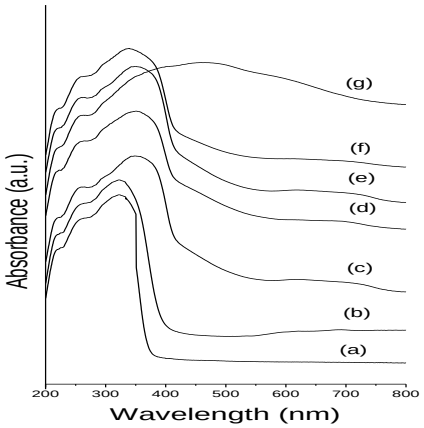

Fig. 3(a–g) UV–VIS-DR spectra of (a) Pure TiO_2, (b) 1 wt.% Sb/TiO_2, (c) 3 wt.% Sb/TiO_2, (d) 5 wt.% Sb/TiO_2, (e),7 wt.% Sb/TiO_2 (f) 9 wt.% Sb/TiO_2 (g) 11 wt.% Sb/TiO_2

The absorption shifts of the samples toward the longer wavelength increases with increase in the percentage of loaded metal as shown in the Fig. 3(a-g). The calculated band gap of pure TiO_2 is 3.09 eV [29], whereas the band gap is lowered to approximately 2.11 eV after the addition of Sb (III) dopant ions. The Band gap narrowing may be due to the substitution of surface oxygen sites by Sb metal ions on TiO_2 surface [30] or by accumulation of Sb ions on oxygen-deficient sites formed in the grain

boundaries [31].

3.4 Thermal analysis

Fig. 4 shows the thermal evolution of 5 wt.% Sb/TiO_2. Several components, such as physically adsorbed water and residual organic materials coming from the synthesis may be removed before the start of the loss of the sulfate and assigned to different steps in the TG curve. Sharp weight losses are observed in two temperature ranges, the first between 50 and 300□C and the second between 350 and 600□C.

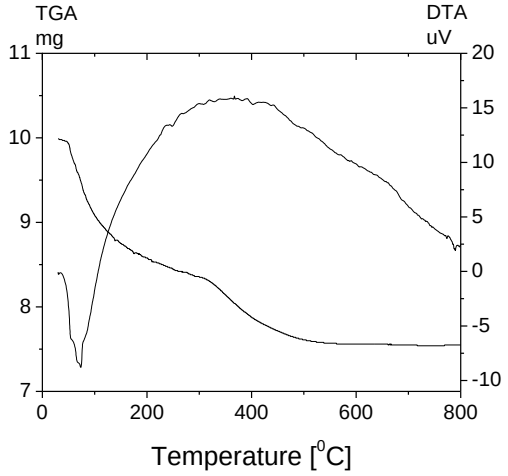

Fig. 4. TG-DTA curve of 5 wt.% Sb-doped TiO_2 sample.

The DTA curve displayed three corresponding valleys for Sb/TiO_2 sample. The first one appeared at about in the temperature region between 50 and 250□C, which is ascribed to water desorption from the samples [32]. The second one emerging at about 400□C could be due to the decomposition of strongly bonded chemical species. The fourth one emerging at about 500□C could be due to the amorphous to anatase transformation of TiO_2 [33].

3.5 FT-IR analysis

The FT-IR spectra of pure TiO_2 and Sb-doped TiO_2 catalysts are shown in Fig. 5(a-g). The FT-IR spectrum of pure TiO_2 shows an absorption band at 1630–1635 cm^{-1}, which is due to the presence of the unassociated H_2O on TiO_2 surface. The broad absorption band at 3800–2500 cm^{-1} reveals a large amount of adsorbed H_2O and surface OH^- groups on the TiO_2 surface [34]. A peak appeared at 730 cm^{-1} corresponded to the Ti–O, Ti–O–Ti from titanium dioxide. The Sb-doped TiO_2 samples (Fig. 5(b-g) shows bands in the range 3600–3000 cm^{-1} related to the presence of hydroxyl groups of TiO_2. The absorption band at 1630–1635 cm^{-1}, indicates the presence of the unassociated H_2O on TiO_2 surface. As samples temperature increased the water desorbed and, correspondently, the associated absorptions decreased up to disappear at 400□C. Generally, the bands in the low-wavenumber region (400-600 cm^{-1}) can be assigned to Ti-O bond vibrations. The FT-IR spectra of the modified samples do not show any band corresponding to the transition metal oxide, which confirms the XRD results.

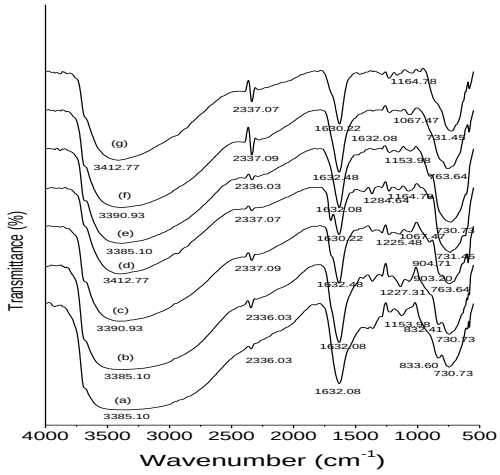

Fig. 5.(a–g) FT-IR spectra of (a) Pure TiO_2, (b) 1 wt.% Sb/TiO_2, (c) 3 wt.% Sb/TiO_2, (d) 5 wt.% Sb/TiO_2, (e),7 wt.% Sb/TiO_2 (f) 9 wt.% Sb/TiO_2 (g) 11 wt.% Sb/TiO_2

3.6 Acidity measurements

NH_3-TPD is used for the evaluation of the surface acidity of the samples. NH_3 desorption peaks were detected between 100 and 600□C, and the total acidity values of the different samples are shown in Table 1. These results indicate that a weak and strong site appears on the surface of these catalysts. Pure TiO_2 shows only low acidity, however, the nature of acid sites is greatly influenced by the amount of the metal incorporated into the lattice and interaction of it with the TiO_2. The TPD study of 2,6-dimethylpyridine was carried out for a comparative evaluation of the Brönsted acidity in the samples [35]. The amount of 2,6-dimethylpyridine desorbed at an appropriate temperature (□ 300□C) due to desorption for Brönsted acid sites of samples are also shown in Table 1. The acidity increases in the case of metal incorporated TiO_2, compared to simple TiO_2 [36].

3.7 Photocatalytic activity

The photocatalytic activities of pure TiO_2, and Sb-doped TiO_2 samples are shown in Fig. 6. In the presence of pure TiO_2, decomposition of MB was not observed. However, in the presence of the Sb- doped TiO_2 samples, the decomposition of MB obviously increased. Among the different concentration levels of Sb (1, 3, 5, 7, 9 and 11wt.%) for Sb/TiO_2 system, 5 wt.% Sb-doped TiO_2 sample exhibited the highest photocatalytic activity under solar light irradiation, only 1-1.5 % of MB remained, and in the case of 3 and 7 wt.% of Sb (III) 3-5 % of MB remained after exposure to solar light for 60 min. While as high as 6-8 % remained in the case of 1, 9, and 11 wt.% of Sb (III). From the observed results it was found that the 5 and 7 wt.% Sb-doped TiO_2 are found to be composite photocatalyst, in this case once optical excitation occurs, the photogenerated electrons can be transferred to the lower-lying conduction band Sb (III), while the holes will accumulate in the valence band of TiO_2, and effectively scavenged by the oxidation of MB, whereas the photogenerated electrons can be transferred into the surface of Sb (III), rather than undergoing bulk recombination. Further, 5 and 7 wt.% Sb-doped TiO_2 samples calcined at 400□C temperature presents a higher surface area and anatase phase. Furthermore, the acid properties of the catalyst are still significant. On the other hand, the acidified surface would lead to the formation of oxygen deficiency upon calcination. The presence of surface oxygen deficiencies can act as capture centers for the photoexcited electrons, and effectively restrain the recombination of electrons and holes, while the surface hydroxyl groups acts as centers for the photocatalytic reaction [37].

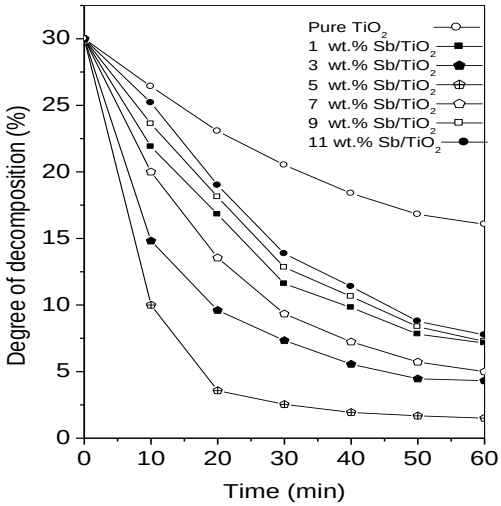

Fig. 6. Rate of decomposition of methyl blue by using (1) pure TiO_2, (2) 1 wt.% Sb/TiO_2, (3) 3 wt.% Sb/TiO_2, (4) 5 wt.% Sb/TiO_2, (5) 7 wt.% Sb/TiO_2,, (6) 9 wt.% Sb/TiO_2, (7) 11 wt.% Sb/TiO_2 calcined at 400°C.

Sb-doped TiO_2 samples shows red-shift in the absorption range compared with pure TiO_2. The existence of oxygen deficiencies, probably located at the anatase-rutile boundary, leads to localized electronic states between the valence and conduction band, shows certain absorption in the visible range. This seems to indicate the absorption could also enhance the efficiency of the photocatalytic reaction since the number of photons participating in the photocatalytic reaction is larger. Furthermore, the higher specific surface area of 5 and 7 wt.% Sb-doped TiO_2 samples implies high adsorption capacity. The conjunction of all this features can lead to the improvement of the photocatalytic efficiency of the 5 and 7 wt.% Sb-doped TiO_2 composite materials.

Conclusion

Sb-doped TiO_2 nanoparticles were prepared by a sol–gel method. The prepared samples were characterized by XRD, HRTEM, FT-IR, XPS, TGA and UV–VIS DRS. The prepared catalyst showed significant photocatalytic activity toward solar light. The smaller particle size and higher concentration of anatase phase contributed to high photocatalytic activity. The catalyst prepared with 5 wt.% antimony containing TiO_2 showed maximum photocatalytic activity in solar light within one hour. The above findings could be helpful for further development of more efficient titanium dioxide photocatalyst.

References

[1] M. Liu, L.Y. Piao, W.J. Wang, J. Nanosci. Nanotechnol. 10 (2010) p. 7469.
[2] E. Abdelkader, L. Nadjia, B. Ahmed, Appl. Surf. Sci. 258 (2012) p. 5010.
[3] M. Liu, X. Qiu, M. Miyauchi, K. Hashimoto, Chem. Mater. 23 (2011) p. 5282
[4] A.G. Mailer, P.S. Clegg, J. Colloid Interface Sci. 417 (2014) p. 317.
[5] J.A. Rengifo-Herrera, E. Mielczarski, J. Mielczarski, N.C. Castillo, J. Kiwi, C. Pulgarin, Appl. Catal. B-Environ. 84 (2008) p. 448
[6] W. Li, C. Ni, H. Lin, C.P. Huang, S. Ismat Shah, J. Appl. Phys. 96 (2004) p. 6663.
[7] D.A.H. Hanaor, C.C. Sorrell, J. Mater. Sci. 46 (2011) p. 855
[8] F. Wang, L. Feng, D. Zhang, Q. Tang, D. Feng, J. Alloy. Compd. 611 (2014) p. 125.
[9] L. Kernazhitsky, V. Shymanovska, T. Gavrilko, V. Naumov, V. Kshnyakin, T. Khalyavka, J. Solid State Chem. 198 (2013) p. 511.
[10] M.L. Kaariainen, D.C. Cameron, Thin Solid Films 526 (2012) p. 212.
[11] X. Chen, L. Liu, P.Y. Yu, S.S. Mao, Science 331 (2011) p. 746.
[12] S. Munusamy, R.S.L. Aparna, R.G.S.V. Prasad, Sustain. Chem. Process 1:4 (2013) p. 1.
[13] C. Wang, H. Shi, Y. Li, Appl. Surf. Sci. 257 (2011) p. 6873.
[14] S. Gomez, C.L. Marchena, L. Pizzio, L. Pierella, J. Hazard. Mater. 258– 259 (2013) p. 19.
[15] A.N. Ejhieh, M. Amiri, Powder Technol. 235 (2013) p. 279.
[16] F. Li, Y. Jiang, M. Xia, M. Sun, B. Xue, X. Ren, J. Hazard. Mater. 165 (2009) p. 1219.
[17] J. Zhang, S. Tang, L. Liao, W. Yu, J. Li, F. Seland, G.M. Haarberg, J. Power Sources 267 (2014) p. 706.
[18] B. Karthikeyan, L. Natanapatham, S. Senthilvelan, V.L. Chandraboss, M. Murugavelu, Mat. Sci. Semicon. Proc. 16 (2013) p. 23.
[19] E.S. Baeissa, J. Ind. Eng. Chem. 20 (2014) p. 3761.
[20] H.Y. Lin, Y.S. Chang, Int. J. Hydrogen Energ. 39 (2014) p. 3118.
[21] K.J. Kim, P.B. Kreider, C. Choi, C.H. Chang, H.G. Ahn, RSC Adv., 3 (2013) p. 12702.
[22] K. Maeda, ACS Appl. Mater. Interfaces. 6(3) (2014) p. 2167.
[23] C.C. Hu, J.N. Nian, H. Teng, Sol. Energ. Mat. Sol. C. (2008) p. 1071.
[24] J. Wang, Y. Wang, P. Zhang , D. Zhang, X. Ren, J. Alloy Compd. 610 (2014) p. 308.
[25] J. Xua, Q. Li , M.K. Hansen , E. Christensen , A.L.T. Garcı´ , G. Liu, X. Wanga, N. J. Bjerrum, Int. J. Hydrogen Energ. 37 (2012) p. 18629.
[26] C.C. Pei, W.W.F. Leung, Sep. Purif. Technol. 114 (2013) p. 108.
[27] L. Rizzoa, D. Sanninob, V. Vaianob, O. Saccob, A. Scarpaa, D. Pietrogiacomic, Appl. Catal. B-Environ. 144 (2014) p. 369.
[28] H. Takagi, Y. Fujishiro, M. Awano, J. Mater. Sci. 36 (2001) p. 949.
[29] Y. Lva, L. Yua, H. Huangb, H. Liub, Y. Fengb, J. Alloy. Compd. 488 (2009) p. 314.
[30] R.R. Bhosale, S.R. Pujaria, M.K. Lande, B.R. Arbad, S.B. Pawar, A.B. Gambhire, Appl. Surf. Sci. 261 (2012) p. 835.
[31] T. Ihara, M. Miyoshi, Y. Triyama, O. Marsumato, Appl Catal B 42 (2003) p. 403.
[32] A. Bellifa, L. Pirault-Roy, C. Kappenstein, A. Choukchou-Braham, Bull. Mater. Sci. 37 (2014) p. 669.
[33] C.J. Bodson, S.L. Pirard, R. Pirard, L. Tasseroul, C. Bied, M.W.C. Man, B. Heinrichs, S.D. Lambert, J. Chem. Eng. Mater. Sci. 2 (2014) p. 17.
[34] M.Li, K.N. Hui, K.S. Hui, S.K. Lee, Y.R. Cho, H. Lee, W. Zhou, S. Cho, C.Y.H. Chao, Y. Li, Appl. Catal. B- Environ. 107 (2011) p. 245.
[35] M.V. Dozzi, E. Selli, Catalysts 3 (2013) p. 455.
[36] R.M. de Almeida, F.T.C. Souza, M.A.C. Júnior, N.J.A. Albuquerque, S.P. Meneghetti, M.R. Meneghetti, Catal. Commun., 46 (2014) p. 179.
[37] L. Liu, Y. Li, Aerosol Air Qual Res, 14 (2014) p. 453.